

Article

Interaction Mechanism of RGD Tripeptide on Different Surfaces of Mg and Mg Alloys: A First-Principles Study

Zhe Fang^{1,2,3,*}, Huili Ding², Ping Li², Huijie Qiao², Erjun Liang^{1,*}, Yu Jia^{1,4} and Shaokang Guan^{3,*}

¹ International Laboratory for Quantum Functional Materials of Henan & School of Physics and Microelectronics, Zhengzhou University, Zhengzhou 450001, China

² School of Materials and Chemical Engineering, Zhongyuan University of Technology, Zhengzhou 450007, China

³ School of Materials Science and Engineering, Zhengzhou University, Zhengzhou 450001, China

⁴ Key Laboratory for Special Functional Materials of Ministry of Education, Henan University, Kaifeng 475004, China

* Correspondence: zhefang@zut.edu.cn (Z.F.); ejliang@zzu.edu.cn (E.L.); skguan@zzu.edu.cn (S.G.)

Highlights:

- The adsorption models of RGD on different surfaces of Mg and Mg alloys were set up.
- Alloying elements promoted the adsorption of RGD on different Mg surfaces.
- The ligand covalent bond between RGD and substrate was formed.
- The pronounced localization of electrons of Mg(11 $\bar{2}$ 0) and Mg(10 $\bar{1}$ 1) surfaces improved the adsorption.

Abstract: Functional Arg-Gly-Asp (RGD) tripeptide has a tremendous potential in clinical applications to accelerate the endothelialization of Magnesium (Mg) alloy vascular stent surface. The interaction mechanism of RGD on different surfaces of Mg and Mg alloy is important for promoting the development of Mg alloy vascular stent, yet still unclear. In the present work, first-principles calculation within density functional theory (DFT) was performed to investigate the interaction mechanism. The electron redistribution, effect of alloying elements and changes in the density of states of the adsorption systems were studied. The results revealed that RGD interacted with different surfaces of Mg (0001), Mg(11 $\bar{2}$ 0) and Mg(10 $\bar{1}$ 1) through ligand covalent bond; the pronounced localization of electrons of Mg(11 $\bar{2}$ 0) and Mg(10 $\bar{1}$ 1) surfaces promoted the adsorption of RGD tripeptide compared with that on the Mg(0001) surface; Zn/Y/Nd alloying elements improved the adsorption of RGD. Calculated results could provide insight for the interaction mechanism of biomolecule on the Mg and Mg-based alloy surfaces, and point out some directions for the future experimental efforts.

Keywords: RGD; Mg alloy; different surfaces; first-principles calculation; interaction mechanism



Citation: Fang, Z.; Ding, H.; Li, P.; Qiao, H.; Liang, E.; Jia, Y.; Guan, S. Interaction Mechanism of RGD Tripeptide on Different Surfaces of Mg and Mg Alloys: A First-Principles Study. *Coatings* **2022**, *12*, 1814. <https://doi.org/10.3390/coatings12121814>

Academic Editor: Vincent Ji

Received: 21 October 2022

Accepted: 21 November 2022

Published: 24 November 2022

Publisher's Note: MDPI stays neutral with regard to jurisdictional claims in published maps and institutional affiliations.



Copyright: © 2022 by the authors. Licensee MDPI, Basel, Switzerland. This article is an open access article distributed under the terms and conditions of the Creative Commons Attribution (CC BY) license (<https://creativecommons.org/licenses/by/4.0/>).

1. Introduction

Magnesium (Mg) alloys with good biodegradability, biocompatibility and mechanical compatibility have become a research hotspot in biodegradable vascular stent materials in recent years [1–3]. In the physiological environment, the slow endothelialization process of the endothelial cell on Mg alloys surfaces could lead to inflammation, thrombosis and vascular restenosis, which limits the clinical application of Mg alloys vascular stent [4–6]. In the past decades, the construction of functional biomolecular coatings, such as Arg-Gly-Asp (RGD), Arg-Glu-Asp-Val (REDV) and Tyr-Ile-Gly-Ser-Arg (YIGSR), on the Mg alloys surfaces were considered as an effective strategy to improve the endothelialization process [7–9]. RGD tripeptide sequence was existing in a variety of extracellular matrices and containing specific binding sites with integrin receptors on the surface of endothelial cells (ECs). It had been extensively used for surface modification to promote the adhesion

of ECs and inhibit the blood coagulation [10,11]. Kou et al. [12] pointed out that covalent bonding between carboxyl group and amine group was a preferable method in immobilizing bioactive molecules on the materials' surfaces and developed the PDA/CA-RGD multilayers on Mg-Zn-Y-Nd alloy surface. The in vitro cytocompatibility experiments indicated that the PDA/(CA-RGD)₂ coating not only displayed excellent performance in promoting surface endothelialization, but also provided sustained inhibition effects on SMCs adhesion and proliferation. Schieber et al. [13] concluded that RGD-coated CoCr surfaces induced a significant increase in ECs' adhesion without significantly enhancing SMCs' adhesion. Wang et al. [14] reported that various density combinations of RGD tripeptide and YIGSR in a quantitative and high-throughput manner to obtain surfaces on which ECs exhibited preponderant adhesion over SMCs.

The functional RGD tripeptide coating could significantly improve the endothelialization process, while the interaction mechanism of RGD tripeptide on the different Mg alloys surfaces was still unclear. With the help of the computational simulation, some detailed information about the interaction process of RGD tripeptide on the other material (rather than Mg alloys) surfaces at the atomic scale was obtained. Deguchi et al. [15] noted that RGD tripeptide was the most stable state when two oxygen atoms of carboxyl group in Asp were located very close to the atop sites of Au surface. Höffling et al. [16] reported that the two-coordinate covalent bond between the dipeptide Arg-Cys and Au(111) surface led to a strong interaction via the first-principles study. The amino acids and short peptides preferred to lie flat on the surface with the N and O anions in their functional groups (carboxyl, amine and guanidyl) binding to the Mg atoms [17,18]. Structural and electronic characteristics of RGD tripeptide and cyclophosphamide anticancer drugs were reported and the results indicated the effect of strong hydrogen bond interactions by using density functional theory (DFT) calculations and molecular dynamics (MD) simulations [19].

Another important factor affecting RGD tripeptide adsorption was the properties of different material surfaces, as different processes and surface treatment methods made the material have a polycrystalline surface distribution. The calculated results showed that RGD tripeptide had a higher binding energy on anatase (001) and rutile (010) than the other corresponding surfaces through MD simulations [20]. Zhang et al. [21] concluded that the interaction of RGD tripeptide on the anatase (101) surfaces was stronger than that on the rutile (110) surfaces through the energy analysis. In terms of different Mg surfaces, most studies focused on hydrogen storage properties and mechanical properties of the Mg basal, prismatic and pyramidal surfaces [22–25]. However, the research on the interaction mechanism of RGD tripeptide with different surfaces of Mg and Mg alloys has not been reported in the previous literature.

Based on the above background and the authors' previous studies about the interaction between biomolecules and Mg(0001) surface [17,18,26], the interaction mechanism of RGD with different surfaces of Mg and Mg alloys by the first-principles calculation was proposed in this study. Firstly, the properties of different surfaces (basal (0001), prismatic (10 $\bar{1}$ 0), (11 $\bar{2}$ 0), (21 $\bar{3}$ 0) and pyramidal (10 $\bar{1}$ 1) surfaces) of pure Mg were investigated. Secondly, the adsorption of RGD tripeptide on the pure Mg(0001), Mg(11 $\bar{2}$ 0) and (10 $\bar{1}$ 1) surfaces were calculated, and the effect of alloying elements on the adsorption of RGD tripeptide on different surfaces were analyzed. Finally, the interaction mechanism of RGD tripeptide on different surfaces of Mg and Mg alloys were proposed after studying the electronic properties. The calculated results could provide theoretical support for the selection of surface texture processing methods of biomedical Mg alloys.

2. Computational Methods

The DFT calculations were carried out using the Vienna *Ab initio* Simulation Package (VASP) with the projected augmented wave (PAW) method [27–29]. The exchange-correlation energy was dealing with the Perdew–Burke–Ernzerhof (PBE) functional with the framework of the generalized gradient approximation (GGA) [30]. The optB86b method proposed by Klimesis was adopted for van der Waals (vdW) correction [31,32]. The sur-

face energy (E_{surf}) and work functions of basal (0001), prismatic ($10\bar{1}0$), ($11\bar{2}0$), ($21\bar{3}0$) and pyramidal ($10\bar{1}1$) surfaces of Mg were obtained using periodic boundary conditions with the energy cutoff of 400 eV. A 1×1 supercell with a certain atomic layer thickness in the z-direction was chosen as the surface model, and the thickness of the vacuum layer was 40 Å to ensure the same symmetry between the upper and lower surfaces. The k-point in the Brillouin zone in the direction of the vacuum layer was chosen as 1 and the k-point of atomic layer direction was taken as at least 25. The convergence accuracy of the total energy of the system was 10^{-8} eV, and the convergence criterion of the force was 10^{-4} eV/Å. When calculating the interaction of RGD tripeptide on the Mg surfaces, six atomic layer thickness with the vacuum of 20 Å were chosen as the surface model. The convergence criterion of the force and the electron relaxation energy for the adsorption system were set at 0.02 eV/Å and 10^{-5} eV, respectively. The bottom two layers of Mg atoms were fixed and the remaining Mg atoms and RGD were fully relaxed to the convergence criterion during the optimization of the adsorption systems. The E_{surf} for different number of layers were obtained by using the following equation.

$$E_{surf} = \frac{1}{2A}(E_{slab} - N_{slab}E_{bulk}) \quad (1)$$

where A is the area of the surface; E_{slab} is the energy of the optimized surface; N_{slab} is the number of atoms in the selected surface model; and E_{bulk} is the energy of per atom in the bulk.

The adsorption energy (E_{ads}) of molecules on the substrates were expressed as follows.

$$E_{ads} = E_{mol+sub} - (E_{mol} + E_{sub}) \quad (2)$$

where E_{mol} , E_{sub} and $E_{mol+sub}$ represent the total energy of the optimized RGD, the energy of the substrates and the energy of the stable adsorption systems, respectively.

3. Results and Discussion

3.1. Properties of Different Surfaces of Pure Mg

The surface energy is an important parameter to determine the surface stability of the materials. The thickness of the constructed surface model, which was at least 10 Å, was obtained by adjusting the number of selected Mg atomic layer. The topmost and bottommost surfaces were the same. Configurations of the basal (0001), prismatic ($10\bar{1}0$), ($11\bar{2}0$), ($21\bar{3}0$) and pyramidal ($10\bar{1}1$) surfaces of pure Mg were fully relaxed at the convergence criterion set, as shown in Figure 1.

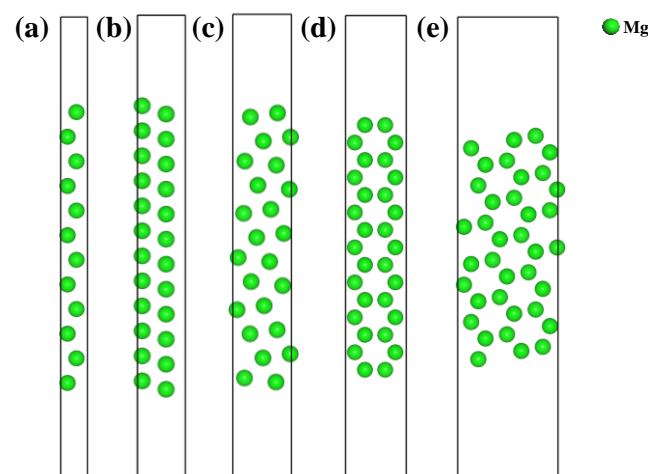


Figure 1. Configurations of different Mg surfaces: (a) basal (0001); (b–d) prismatic ($11\bar{2}0$), ($21\bar{3}0$), ($10\bar{1}0$); and (e) pyramidal ($10\bar{1}1$).

The surfaces with different Miller indices presented different properties due to the orientation of the atomic arrangement. For the configurations of Mg surfaces, six models with gradually increasing thicknesses were selected for each surface, and the E_{surf} of Mg surfaces at different layer thicknesses were calculated according to equation (1), as shown in Figure 2.

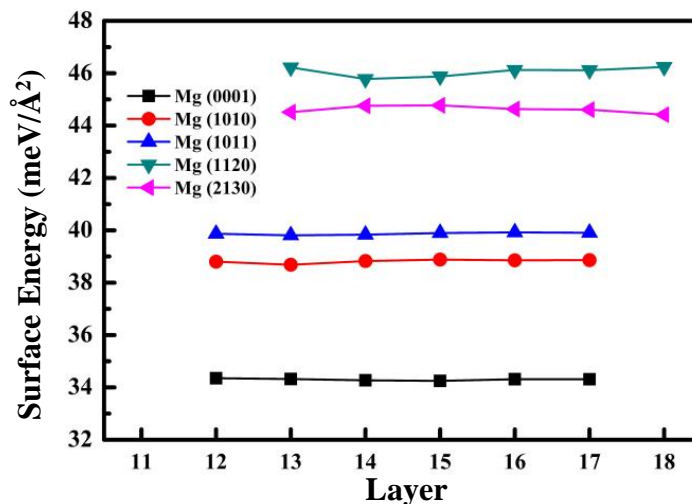


Figure 2. Surface energies of Mg basal (0001), prismatic (1010), (1120), (2130) and pyramidal (1011) surfaces.

As seen in Figure 2, the fluctuations in surface energy are small as the thickness gradually increases, which shows a good convergence. Mg(0001) and Mg(1120) surfaces had the lowest and the highest E_{surf} , respectively. The order of E_{surf} for the above different surfaces was (1120) > (2130) > (1011) > (1010) > (0001). Work function was the required energy to move an electron from the Fermi energy level to vacuum at 0 K, and it was also investigated by Equation (3). The calculated work function of different Mg surfaces was depicted in Table 1.

$$\Phi = V_{vacuum} - E_{fermi} \tag{3}$$

where V_{vacuum} is the vacuum electrostatic potential; and E_{fermi} is the Fermi energy level.

Table 1. Surface energy and work function of different surfaces of Mg.

Surface	Surface Energy(meV/Å²)		Work Function (eV)	
	This Work	Other Works	This Work	Other Works
0001	34.30	34.37 [33], 34.61 [34]	3.69	3.70 [34], 3.80 [35]
1010	38.81	39.90 [34]	3.61	3.60 [34], 3.64 [36]
1011	39.87	40.90 [34]	3.69	3.80 [34], 3.70 [34]
1120	45.94	45.70 [34]	3.66	4.00 [34]
2130	44.61	46.62 [36]	3.49	3.49 [36]

As seen in Table 1, the E_{surf} and Φ of Mg(0001) surface were 34.30 meV/Å² and 3.69 eV, respectively, which were in good agreement with the Refs. [33,34]. Compared with other Mg surfaces (1010), (1120), (2130) and (1011), Mg(0001) surface had the smallest E_{surf} and the largest work function, which means this surface was the most stable one. With the larger surface energy and lower work function, the prismatic (1010), (1120), (2130) and pyramidal (1011) surfaces were more electronically active and were prone to chemical reactions once stimulated by external conditions.

3.2. Adsorption of RGD on Different Surfaces of Pure Mg and Mg Alloy

3.2.1. Adsorption of RGD on Different Surfaces of Pure Mg

From the optimized stable adsorption structures of biomolecules in Refs. [17,18], it was clear that the strongest interaction occurred when the biomolecules were adsorbed in a flat lying manner on the Mg(0001) surfaces of Mg and Mg alloys. RGD had three potential metal-binding groups: guanidyl ($-\text{CN}_3\text{H}_4$), amino ($-\text{NH}_2$), and carboxyl ($-\text{COOH}$). These functional groups could be used as monodentate or bidentate ligands to make RGD more easily adsorbed on the surfaces. Many adsorption configurations of RGD on the (0001), $(11\bar{2}0)$ and $(10\bar{1}1)$ surfaces were optimized. The adsorption regularity showed that the most stable configurations occurred when functional groups bounded to the surface as much as possible. In addition, the stabilities of the most stable configurations at room temperature were checked by using ab initio molecular dynamics simulations [18], and the results showed that they were stable. The most stable adsorption configurations of RGD on the Mg(0001), Mg($11\bar{2}0$) and Mg($10\bar{1}1$) surfaces were shown in Figure 3.

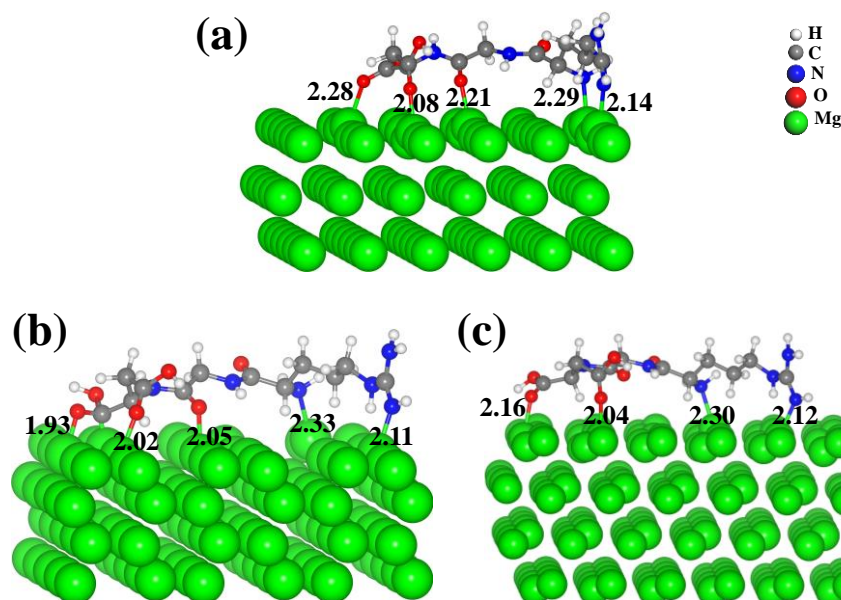


Figure 3. Stable adsorption configurations of RGD on the surfaces: (a) Mg(0001), (b) Mg($11\bar{2}0$) and (c) Mg($10\bar{1}1$).

According to equation (2), the E_{ads} of RGD on the Mg(0001), Mg($11\bar{2}0$) and Mg($10\bar{1}1$) surfaces were -3.24 eV, -4.44 eV and -3.32 eV, respectively. As shown in Figure 3, RGD was anchored to the Mg(0001), Mg($11\bar{2}0$) and Mg($10\bar{1}1$) surfaces via amino, carboxyl and guanidinium functional groups. The calculated E_{ads} of RGD on the Mg($11\bar{2}0$) and Mg($10\bar{1}1$) surfaces were 1.20 eV and 0.08 eV higher than that of on the Mg(0001) surface (-3.24 eV) [25], respectively. It was much easier for RGD to be adsorbed on the Mg($11\bar{2}0$) and Mg($10\bar{1}1$) surfaces compared with that on the Mg(0001) surface. For the stable adsorption configurations, the O-Mg and N-Mg bond lengths ranges of RGD on the pure Mg surfaces were 1.93–2.16 Å and 2.11–2.33 Å, respectively. The optimized O-Mg and N-Mg bond lengths were very close to the theoretical bond lengths of the formation of covalent bonds of N-Mg and O-Mg (2.11 Å and 2.09 Å) [37], indicating a ligand covalent bond of RGD on the pure Mg surfaces.

3.2.2. Effect of Zn, Y and Nd Alloying Elements on the Adsorption of RGD on Different Mg Alloys Surfaces

To analyze the effects of Zn, Y and Nd alloying elements, the adsorption of RGD on the (0001), $(11\bar{2}0)$ and $(10\bar{1}1)$ surfaces of Mg alloys were further calculated. Mg-Zn (1%, 2% and 3%), Mg-Y (1%) and Mg-Nd (1%) were considered in the present calculations. Note

that the alloy concentrations should be connected with the number of Zn, Y and Nd in the respective supercells as well as on the symmetry of the primitive cells [38]. The substitution alloying elements were located at the first-topmost layer of Mg alloys surfaces to make the influence of alloying elements more evident. The initial configurations of RGD on the Mg alloys surfaces were the same as that of RGD on the pure Mg(0001), Mg(11 $\bar{2}$ 0) and (10 $\bar{1}$ 1) surfaces, as shown in Figure 3. The stable adsorption configurations of RGD on different surfaces of Mg alloys were fully optimized to the convergence criterion set. From the optimized structures, the surface charge redistribution was influenced by the addition of alloying elements which affected the following adsorption process. It was noticed that RGD tripeptide was attracted toward Y/Nd but repelled by Zn element as the electronegativity of Y (1.22) is smaller than that of Mg (1.31) while the electronegativity of Zn (1.65) was greater than that of Mg [17,39]. Figure 4 shows the optimized adsorption configurations of RGD on the Zn-, Y- and Nd-doped surfaces.

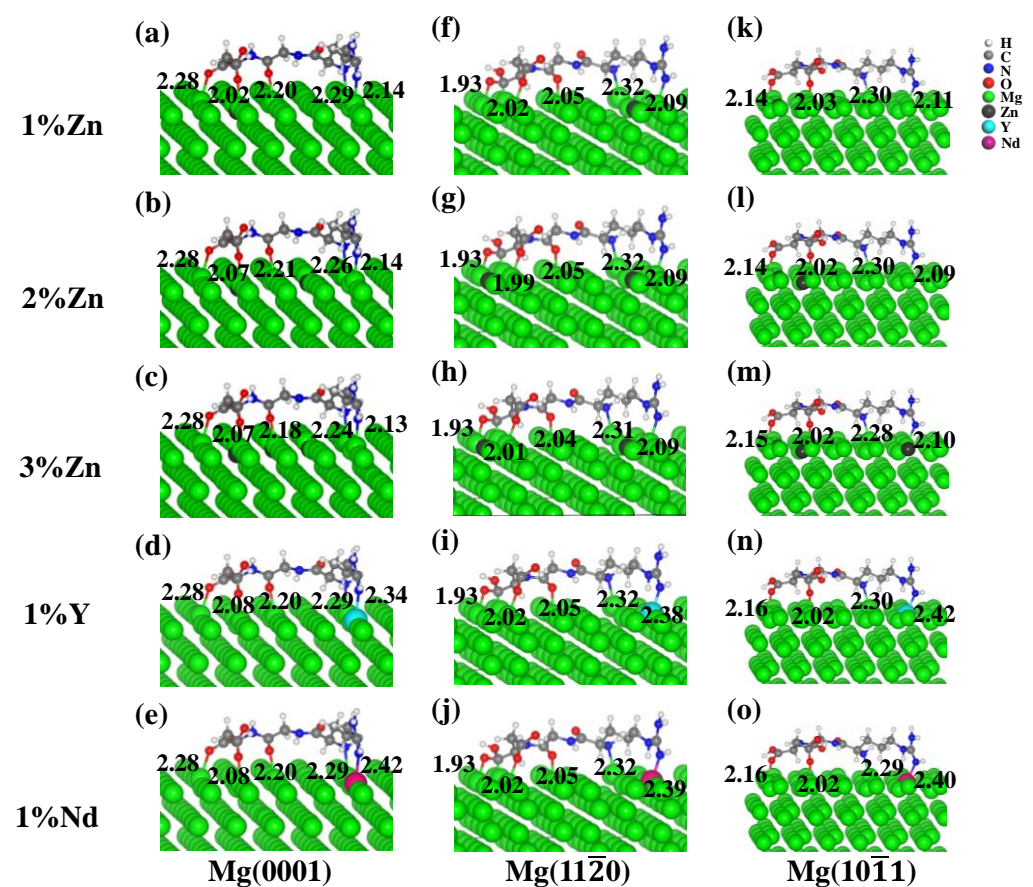


Figure 4. Optimized adsorption configurations of RGD on the Zn-, Y- and Nd-doped surfaces: (a–e) Mg(0001) surfaces, (f–j) Mg(11 $\bar{2}$ 0) surfaces and (k–o) Mg(10 $\bar{1}$ 1) surfaces. The bond lengths (in Å) are also listed.

For the Zn-doped surfaces, RGD preferred to be adsorbed on the Mg atom around the Zn atom; while for Y- and Nd-doped cases, RGD preferred to be adsorbed on the Y or Nd atom, as shown in Figure 4. It was easier for RGD tripeptide to be adsorbed on the neighbor site of the Zn-doped position, and on the top site of Y-/Nd-doped atom rather than the neighbor site of Y/Nd atom. The corresponding bond lengths on the Zn-doped Mg alloys surfaces were about 0.01–0.03 Å lower than that on the pure Mg surfaces. For Y- and Nd-doped Mg alloy surfaces, the range of bond lengths were 2.34–2.40 Å and 2.39–2.42 Å, respectively, which were very close to the sum of the theoretical covalent radii bond lengths of 2.40 Å and 2.43 Å [37].

Table 2 shows the E_{ads} of RGD on the (0001), (11 $\bar{2}$ 0) and (10 $\bar{1}$ 1) surfaces of Mg alloys. Compared with the calculated results of RGD on the clean Mg(0001), Mg(11 $\bar{2}$ 0) and Mg(10 $\bar{1}$ 1) surfaces, the addition of the alloying elements enhanced the adsorption process. The E_{ads} of RGD on the 1%, 2% and 3% Zn-doped Mg alloys surfaces increased about 0.29~0.49 eV, 0.03~0.11 eV and 0.19~0.22 eV, respectively. The promoting effect of Zn alloying element was enhanced with the increase of Zn content. For Y-/Nd-doped Mg alloys surfaces, The E_{ads} of RGD on different surfaces of Mg alloys were significantly increased due to the more active extranuclear electrons. The rank of the E_{ads} for different surfaces was (11 $\bar{2}$ 0) > (10 $\bar{1}$ 1) > (0001). With the addition of Zn/Y/Nd alloying elements, new ligand covalent bonds between RGD tripeptide and Mg alloys' surfaces were formed, and alloying elements improved the adsorption process.

Table 2. E_{ads} of RGD on the Mg and Mg alloys surfaces (eV).

Mg Surfaces	Pure	1%Y	1%Nd	1%Zn	2%Zn	3%Zn
Mg(0001)	−3.24	−3.89	−4.03	−3.53	−3.64	−3.73
Mg(11 $\bar{2}$ 0)	−4.44	−5.09	−4.91	−4.47	−4.49	−4.55
Mg(10 $\bar{1}$ 1)	−3.32	−3.56	−3.47	−3.51	−3.52	−3.54

3.3. Electronic Properties of RGD on Mg and Mg-Based Alloy Surfaces

To further understand the interaction properties of the RGD tripeptide on different surfaces of Mg and Mg alloys surfaces, the electronic structure properties of different Mg surfaces were firstly investigated. The projected density of states (PDOS) of the most superficial atoms in the different Mg surfaces, as well as the individual Mg atoms in the bulk structure, are shown in Figure 5.

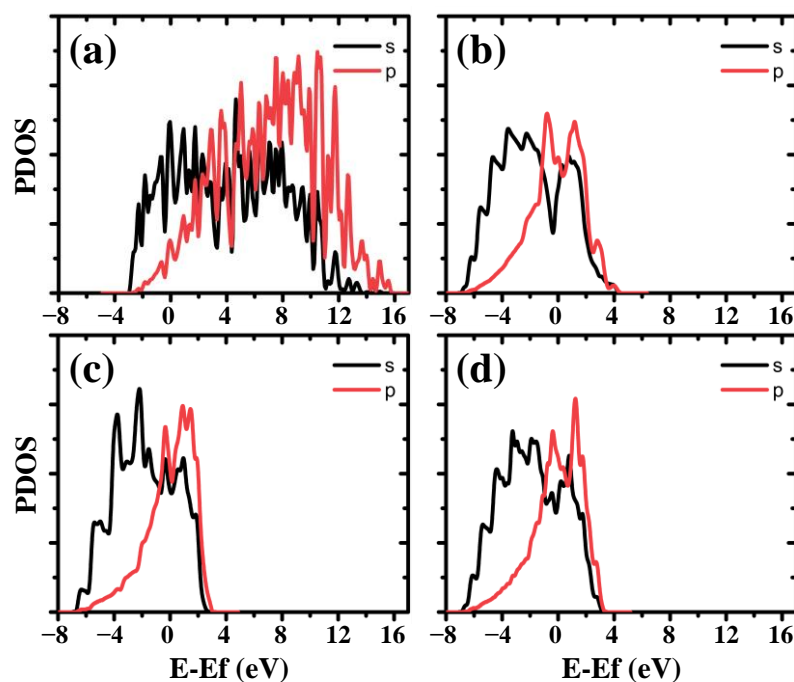


Figure 5. PDOS of a single Mg atom in the (a) Mg bulk structure, (b) the topmost layer of Mg(0001) surface, (c) the topmost layer of Mg(11 $\bar{2}$ 0) surface, and (d) the topmost layer of Mg(10 $\bar{1}$ 1) surface. The Fermi level is set at 0 eV.

Figure 5a shows that the PDOS of the bulk Mg atom is mainly distributed in the range $-4.90\sim 15.90$ eV. The PDOS of the most superficial Mg atoms were mainly distributed in the range of $-7.10\sim 4.40$ eV for the (0001), (11 $\bar{2}$ 0) and (10 $\bar{1}$ 1) surfaces, as depicted in Figure 5b–d. The variation of the electronic density of states of the most superficial Mg

atoms in the (0001), (11 $\bar{2}$ 0) and (10 $\bar{1}$ 1) surfaces was essentially the same compared with the bulk structure. The most noticeable difference between the bulk and surfaces were the downward shift of the *sp* states to the lower energies due to the redistribution of the electrons during surface optimization. Figure 6 shows the charge density distributions of different Mg surfaces. It could be observed that the surface charge density distribution was relatively uniform for the Mg(0001) surface, while the surface charge density distribution of Mg(11 $\bar{2}$ 0) and Mg(10 $\bar{1}$ 1) surfaces were more localized. Mg(11 $\bar{2}$ 0) surface had the most pronounced localization of electrons, and it was relatively active to adsorb RGD. This was one of the reasons that for its larger surface energy and larger E_{ads} of RGD.

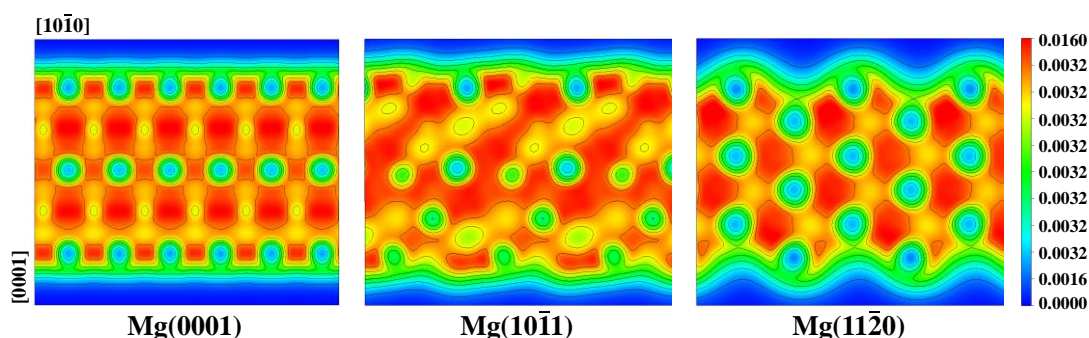


Figure 6. Surface charge density distribution of Mg(0001), Mg(10 $\bar{1}$ 1) and Mg(11 $\bar{2}$ 0).

To analyze the interaction mechanism of RGD on the Mg(11 $\bar{2}$ 0) and Mg(10 $\bar{1}$ 1) surfaces, the changes of electronic structures (see Figures 7 and 8) were investigated through PDOS, and the charge density difference ($\Delta\rho$) was calculated by Equation (4). It should be pointed out that the interaction mechanism of RGD on the Mg(0001) was proposed by our previous paper [17].

$$\Delta\rho = \rho_{mol+surf} - (\rho_{mol} + \rho_{surf}) \quad (4)$$

where $\rho_{mol+surf}$ is the total charge density of the optimized adsorbate–substrate systems, ρ_{mol} is the charge density of RGD without surface, and ρ_{surf} is the charge density of different Mg and Mg alloy surfaces, respectively.

As displayed in Figure 7, the highest occupied molecular orbital (HOMO) and the lowest unoccupied molecular orbital (LUMO) were attributed to the *p* orbitals of the N and O atoms in the functional groups of RGD, which were the active sites for adsorption. The most noticeable difference between the before (Figure 7a–c) and after adsorptions (Figure 7d–f) was the downward shift of the *sp* states of the O and N atoms. After adsorptions, the intensity of O and N states became weaker, as shown in Figure 7d,e, respectively. For the Mg atoms bound with O atoms, the Mg(s) states simultaneously showed a new peak at the -4.60 eV position, indicating the formation of a new chemical bond between RGD and the Mg surface, as shown in Figure 7e,f. For the Mg atoms bound with N atoms, the Mg(s) states appeared at the energy about -4.60 and -6.10 eV, indicating the lone pair electrons of N(*p*) donating to the Mg, as shown in Figure 7e,f.

Significant changes were investigated for the PDOS of RGD tripeptide on the Mg (10 $\bar{1}$ 1) surface, comparing the before adsorption in Figure 8a–c with the corresponding adsorption state in Figure 8d–f. A new peak appeared at the -5.20 eV position for the chemical bond formation of O–Mg atoms. The new peak appeared at -4.30 eV position for the binding process of N–Mg atoms, and electrons in *py* and *pz* orbits had also been redistributed to obtain a more stable state. Interactions of N–Mg atoms was slightly weakened compared with the results of RGD tripeptide on the Mg(11 $\bar{2}$ 0) surface.

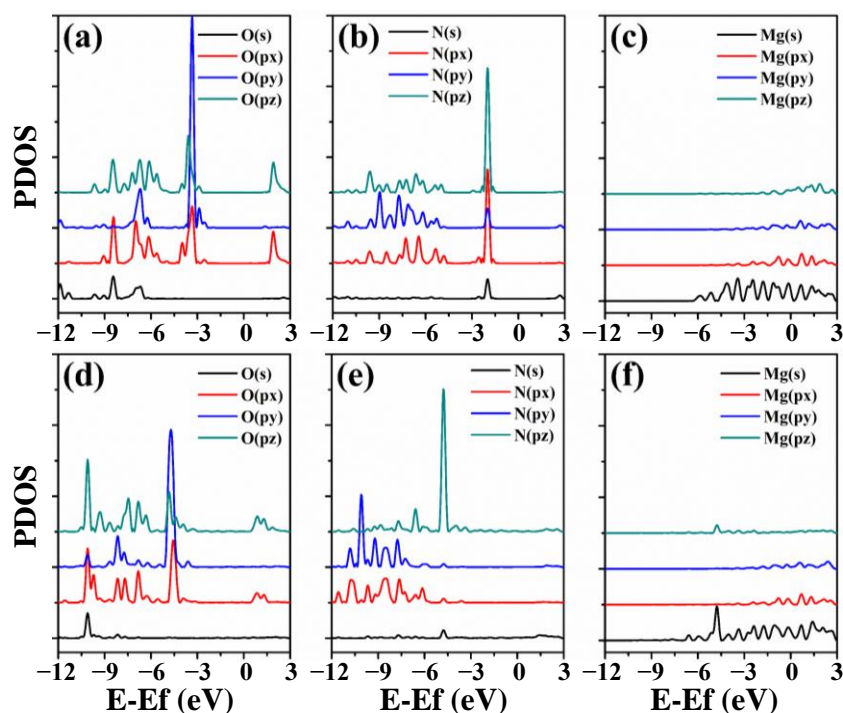


Figure 7. PDOS of the binding atoms on the Mg (11 $\bar{2}$ 0) surface: (a) three O atoms, (b) two N atoms, and (c) five Mg atoms before adsorption; (d–f) are the PDOS of the corresponding atoms after adsorption. The energy zero is set to the Fermi level.

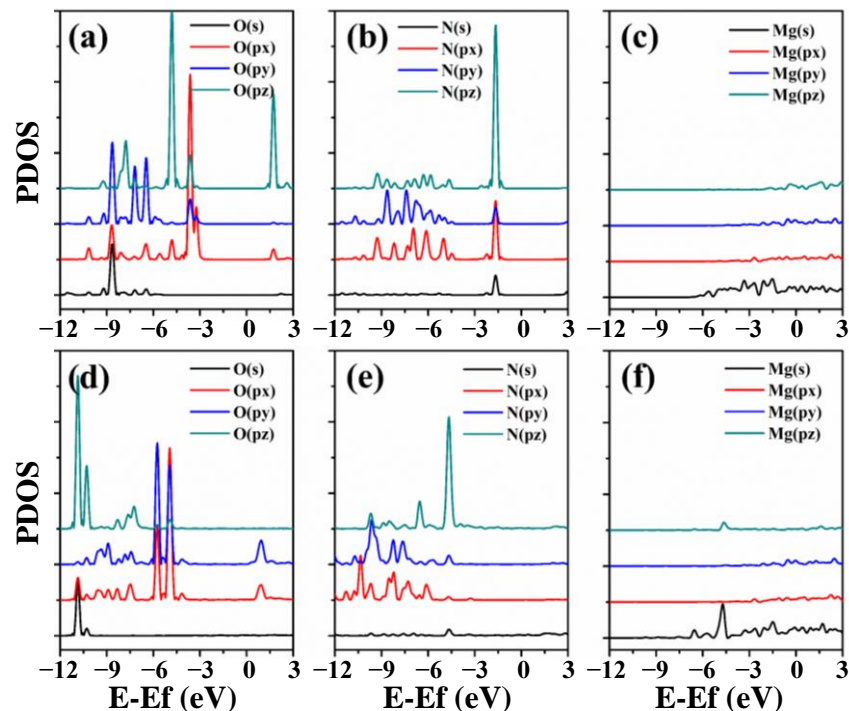


Figure 8. PDOS of the binding atoms on the Mg (10 $\bar{1}$ 1) surface: (a) two O atoms, (b) two N atoms, and (c) four Mg atoms before adsorption; (d–f) are the PDOS of the corresponding atoms after adsorption. The energy zero is set to the Fermi level.

For a clear description of the charge redistribution after the adsorption, the charge density differences for the adsorptions of RGD on the Mg(0001), Mg(11 $\bar{2}$ 0) and Mg(10 $\bar{1}$ 1) surface were calculated to investigate the interactions, as depicted in Figure 9. The yellow

and light cyan regions indicated the interactions between RGD and different surfaces due to the rearrangement of electrons. A significant accumulation of charge density occurred between RGD and different Mg surfaces, as shown in the yellow regions of O-Mg and N-Mg binding atoms in Figure 9. The new chemical bonds were described from the 2D and 3D coordinates according to the PDOS analysis and charge density differences.

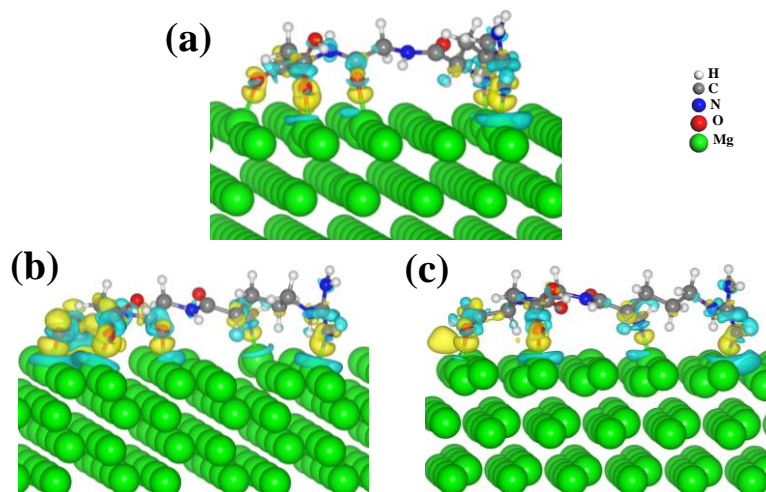


Figure 9. Charge density difference of RGD on the (a) Mg(0001), (b) Mg(11 $\bar{2}$ 0) and (c) Mg(10 $\bar{1}$ 1) surfaces. The values of the isosurfaces are $\pm 0.03 \text{ e}/\text{\AA}^3$, and the yellow and light cyan isosurfaces indicate the accumulation and depletion of charge density.

The PDOS and charge density differences of RGD tripeptide on different surfaces of Mg alloys showed a similar regularity. The intensity of the binding peak was influenced by the addition of the Zn/Y/Nd alloying elements, while the bonding nature was still the ligand covalent bond. Electron redistribution was the driving force behind the changes observed in the structure of RGD tripeptide on different surfaces of Mg and Mg alloys. The calculated results concluded that this driving force made it easy for the lone pair of electrons of N/O to share bonding with the Mg atom to form the ligand covalent bond.

4. Conclusions

In this study, the influences of different surfaces and different alloying elements were investigated, and the interaction mechanism of RGD tripeptide on different surfaces of Mg and Mg alloys surfaces were analyzed. The conclusions can be drawn as follows.

- (1) The order of E_{surf} for the above different surfaces was $(11\bar{2}0) > (21\bar{3}0) > (10\bar{1}1) > (10\bar{1}0) > (0001)$. The higher surface energy made it much easier to interact with RGD, and the order of E_{ads} was $\Delta E(11\bar{2}0) > \Delta E(10\bar{1}1) > \Delta E(0001)$.
- (2) For Mg alloys surfaces, the addition of Zn/Y/Nd alloying elements improved the association of RGD tripeptide with the different Mg alloys surfaces. The E_{ads} also gradually increased with the increase of alloying element Zn content.
- (3) RGD tripeptide was bonded to the (0001), (11 $\bar{2}$ 0) and (10 $\bar{1}$ 1) surfaces of Mg through the ligand covalent bond. The pronounced localization of electrons of Mg(11 $\bar{2}$ 0) and Mg(10 $\bar{1}$ 1) surfaces promoted the adsorption of RGD tripeptide compared with that on the Mg(0001) surface. The calculated results provide insight for the interaction mechanism of RGD tripeptide on the Mg and Mg-based alloy surfaces, and also point out some directions for the design of functional biomolecular coatings.

Author Contributions: Conceptualization, Z.F. and H.D.; methodology, P.L.; software, Z.F.; formal analysis, H.D.; resources, S.G.; data curation, P.L.; writing—original draft preparation, Z.F.; writing—review and editing, Y.J.; visualization, H.Q.; supervision, Y.J. and E.L.; funding acquisition, S.G. All authors have read and agreed to the published version of the manuscript.

Funding: The authors are very grateful for the financial support including the National Key Research and Development Program of China (2021YFC2400700), the Key Projects of the Joint Fund of the National Natural Science Foundation of China (U1804251) and Youth Fund Project of Zhongyuan University of Technology (K2022QN026).

Institutional Review Board Statement: Not applicable.

Informed Consent Statement: Not applicable.

Data Availability Statement: Not applicable.

Acknowledgments: The calculations were supported by National Supercomputing Center in Zhengzhou.

Conflicts of Interest: The authors declare no conflict of interest.

References

1. Zhang, Z.-Q.; Yang, Y.-X.; Li, J.-A.; Zeng, R.-C.; Guan, S.-K. Advances in coatings on magnesium alloys for cardiovascular stents—A review. *Bioact. Mater.* **2021**, *6*, 4729–4757. [\[CrossRef\]](#)
2. Wang, H.; Bai, M.; Yuan, H.; Hou, Y.; Liu, Y.; Fang, Z.; Sun, Y.; Wang, J.; Zhu, S.; Guan, S. Zn content mediated fibrinogen adsorption on biodegradable Mg-Zn alloys surfaces. *J. Magnes. Alloy.* **2021**, *9*, 2145–2154. [\[CrossRef\]](#)
3. Li, M.; Jiang, M.; Gao, Y.; Zheng, Y.; Liu, Z.; Zhou, C.; Huang, T.; Gu, X.; Li, A.; Fang, J.; et al. Current status and outlook of biodegradable metals in neuroscience and their potential applications as cerebral vascular stent materials. *Bioact. Mater.* **2022**, *11*, 140–153. [\[CrossRef\]](#)
4. Cheon, K.-H.; Park, C.; Kang, M.-H.; Park, S.; Kim, J.; Jeong, S.-H.; Kim, H.-E.; Jung, H.-D.; Jang, T.-S. A combination strategy of functionalized polymer coating with Ta ion implantation for multifunctional and biodegradable vascular stents. *J. Magnes. Alloy.* **2021**, *9*, 2194–2206. [\[CrossRef\]](#)
5. Wang, P.; Liu, J.; Luo, X.; Xiong, P.; Gao, S.; Yan, J.; Li, Y.; Cheng, Y.; Xi, T. A tannic acid-modified fluoride pre-treated Mg-Zn-Y-Nd alloy with antioxidant and platelet-repellent functionalities for vascular stent application. *J. Mater. Chem. B* **2019**, *7*, 7314–7325. [\[CrossRef\]](#)
6. Zong, J.; He, Q.; Liu, Y.; Qiu, M.; Wu, J.; Hu, B. Advances in the development of biodegradable coronary stents: A translational perspective. *Mater. Today Bio* **2022**, *16*, 100368. [\[CrossRef\]](#)
7. Wang, P.; Xiong, P.; Liu, J.; Gao, S.; Xi, T.; Cheng, Y. A silk-based coating containing GREDVY peptide and heparin on Mg-Zn-Y-Nd alloy: Improved corrosion resistance, hemocompatibility and endothelialization. *J. Mater. Chem. B* **2018**, *6*, 966–978. [\[CrossRef\]](#)
8. Liu, J.; Wang, P.; Chu, C.-C.; Xi, T. A novel biodegradable and biologically functional arginine-based poly(ester urea urethane) coating for Mg-Zn-Y-Nd alloy: Enhancement in corrosion resistance and biocompatibility. *J. Mater. Chem. B* **2017**, *5*, 1787–1802. [\[CrossRef\]](#) [\[PubMed\]](#)
9. Yao, S.; Cui, J.; Chen, S.; Zhou, X.; Li, J.; Zhang, K. Extracellular Matrix Coatings on Cardiovascular Materials—A Review. *Coatings* **2022**, *12*, 1039. [\[CrossRef\]](#)
10. Li, Y.; McRobb, L.S.; Khachigian, L.M. Inhibition of intimal thickening after vascular injury with a cocktail of vascular endothelial growth factor and cyclic Arg-Gly-Asp peptide. *Int. J. Cardiol.* **2016**, *220*, 185–191. [\[CrossRef\]](#) [\[PubMed\]](#)
11. Tugulu, S.; Silacci, P.; Stergiopoulos, N.; Klok, H.-A. RGD—Functionalized polymer brushes as substrates for the integrin specific adhesion of human umbilical vein endothelial cells. *Biomaterials* **2007**, *28*, 2536–2546. [\[CrossRef\]](#) [\[PubMed\]](#)
12. Kou, F.; Liu, C.; Wang, L.; Yasin, A.; Li, J.; Guan, S. Fabrication of Citric Acid/RGD Multilayers on Mg-Zn-Y-Nd Alloy via Layer-by-Layer Self-Assembly for Promoting Surface Biocompatibility. *Adv. Mater. Interfaces* **2021**, *8*, 2002241. [\[CrossRef\]](#)
13. Schieber, R.; Mas-Moruno, C.; Lasserre, F.; Roa, J.J.; Ginebra, M.-P.; Mücklich, F.; Pegueroles, M. Effectiveness of Direct Laser Interference Patterning and Peptide Immobilization on Endothelial Cell Migration for Cardio-Vascular Applications: An In Vitro Study. *Nanomaterials* **2022**, *12*, 1217. [\[CrossRef\]](#)
14. Wang, C.; Hao, H.; Wang, J.; Xue, Y.; Huang, J.; Ren, K.; Ji, J. High-throughput hyaluronic acid hydrogel arrays for cell selective adhesion screening. *J. Mater. Chem. B* **2021**, *9*, 4024–4030. [\[CrossRef\]](#)
15. Deguchi, S.; Hakamada, M.; Mabuchi, M. Adsorption of RGD Tripeptide on Au (111) Surface. *Mater. Trans.* **2019**, *60*, 1711–1715. [\[CrossRef\]](#)
16. Höfiling, B.; Ortman, F.; Hannewald, K.; Bechstedt, F. Single cysteine adsorption on Au(110): A first-principles study. *Phys. Rev. B* **2010**, *81*. [\[CrossRef\]](#)
17. Fang, Z.; Wang, J.; Zhu, S.; Yang, X.; Jia, Y.; Sun, Q.; Guan, S. A DFT study of the adsorption of short peptides on Mg and Mg-based alloy surfaces. *Phys. Chem. Chem. Phys.* **2018**, *20*, 3602–3607. [\[CrossRef\]](#)
18. Fang, Z.; Wang, J.; Yang, X.; Sun, Q.; Jia, Y.; Liu, H.; Xi, T.; Guan, S. Adsorption of arginine, glycine and aspartic acid on Mg and Mg-based alloy surfaces: A first-principles study. *Appl. Surf. Sci.* **2017**, *409*, 149–155. [\[CrossRef\]](#)
19. Nikfar, Z.; Shariatnia, Z. The RGD tripeptide anticancer drug carrier: DFT computations and molecular dynamics simulations. *J. Mol. Liq.* **2019**, *281*, 565–583. [\[CrossRef\]](#)

20. Zhang, H.-P.; Lu, X.; Fang, L.-M.; Weng, J.; Huang, N.; Leng, Y. Molecular dynamics simulation of RGD peptide adsorption on titanium oxide surfaces. *J. Mater. Sci. Mater. Electron.* **2008**, *19*, 3437–3441. [[CrossRef](#)]
21. Zhang, H.-P.; Lu, X.; Leng, Y.; Watari, F.; Weng, J.; Feng, B.; Qu, S. Effects of aqueous environment and surface defects on Arg-Gly-Asp peptide adsorption on titanium oxide surfaces investigated by molecular dynamics simulation. *J. Biomed. Mater. Res. Part A* **2011**, *96A*, 466–476. [[CrossRef](#)] [[PubMed](#)]
22. Ouyang, L.; Tang, J.; Zhao, Y.; Wang, H.; Yao, X.; Liu, J.; Zhu, M. Express penetration of hydrogen on Mg(10 $\bar{1}$ 0) along the close-packed-planes. *Sci. Rep.* **2015**, *5*, 10776. [[CrossRef](#)] [[PubMed](#)]
23. Tang, J.J.; Ye, J.H.; Fang, Y.X.; Lin, Z.; Zhao, Y.J. Transition metal substitution on Mg(10 $\bar{1}$ 0) and Mg(0001) surfaces for improved hydrogenation and dehydrogenation: A systematic first-principles study. *Appl. Surf. Sci.* **2019**, *479*, 626–633. [[CrossRef](#)]
24. Wang, Z.; Guo, X.; Wu, M.; Sun, Q.; Jia, Y. First-principles study of hydrogen dissociation and diffusion on transition metal-doped Mg(0001) surfaces. *Appl. Surf. Sci.* **2014**, *305*, 40–45. [[CrossRef](#)]
25. Banerjee, S.; Pillai, C.G.S.; Majumder, C. First-principles study of the H₂ interaction with transition metal (Ti, V, Ni) doped Mg(0001) surface: Implications for H-storage materials. *J. Chem. Phys.* **2008**, *129*, 174703. [[CrossRef](#)] [[PubMed](#)]
26. Fang, Z.; Zhao, Y.; Wang, H.; Wang, J.; Zhu, S.; Jia, Y.; Cho, J.-H.; Guan, S. Influence of surface charge density on ligand-metal bonding: A DFT study of NH₃ and HCOOH on Mg (0 0 0 1) surface. *Appl. Surf. Sci.* **2019**, *470*, 893–898. [[CrossRef](#)]
27. Kresse, G.; Furthmüller, J. Efficiency of ab-initio total energy calculations for metals and semiconductors using a plane-wave basis set. *Comput. Mater. Sci.* **1996**, *6*, 15–50. [[CrossRef](#)]
28. Kresse, G.; Furthmüller, J. Efficient iterative schemes for ab initio total-energy calculations using a plane-wave basis set. *Phys. Rev. B* **1996**, *54*, 11169–11186. [[CrossRef](#)] [[PubMed](#)]
29. Blöchl, P.E. Projector augmented-wave method. *Phys. Rev. B Condens. Matter Mater. Phys.* **1994**, *50*, 17953–17979. [[CrossRef](#)] [[PubMed](#)]
30. Perdew, J.P.; Burke, K.; Ernzerhof, M. Generalized gradient approximation made simple. *Phys. Rev. Lett.* **1996**, *77*, 3865. [[CrossRef](#)] [[PubMed](#)]
31. Klimes, J.; Bowler, D.; Michaelides, A. Van der Waals density functionals applied to solids. *Phys. Rev. B* **2011**, *83*, 195131. [[CrossRef](#)]
32. Lüder, J.; Sanyal, B.; Eriksson, O.; Puglia, C.; Brena, B. Comparison of van der Waals corrected and sparse-matter density functionals for the metal-free phthalocyanine/gold interface. *Phys. Rev. B* **2014**, *89*, 045416. [[CrossRef](#)]
33. Lee, J.-Y.; Punkkinen, M.; Schönecker, S.; Nabi, Z.; Kádas, K.; Zólyomi, V.; Koo, Y.; Hu, Q.-M.; Ahuja, R.; Johansson, B.; et al. The surface energy and stress of metals. *Surf. Sci.* **2018**, *674*, 51–68. [[CrossRef](#)]
34. Lautar, A.K.; Kopač, D.; Rejec, T.; Bančič, T.; Dominko, R. Morphology evolution of magnesium facets: DFT and KMC simulations. *Phys. Chem. Chem. Phys.* **2018**, *21*, 2434–2442. [[CrossRef](#)] [[PubMed](#)]
35. Wachowicz, E.; Kiejna, A. Bulk and surface properties of hexagonal-close-packed Be and Mg. *J. Physics: Condens. Matter* **2001**, *13*, 10767–10776. [[CrossRef](#)]
36. Ji, D.-P.; Zhu, Q.; Wang, S.-Q. Detailed first-principles studies on surface energy and work function of hexagonal metals. *Surf. Sci.* **2016**, *651*, 137–146. [[CrossRef](#)]
37. Sargent, W. *Table of Periodic Properties of the Elements*; Sargent-Welch Scientific: Skokie, IL, USA, 1980.
38. Evtimova, J.; Drioli, E.; De Luca, G. A density functional theory study of hydrogen occupation in VNiT_i alloys used for dense metal membranes. *J. Alloys Compd.* **2016**, *665*, 225–230. [[CrossRef](#)]
39. Allred, A. Electronegativity values from thermochemical data. *J. Inorg. Nucl. Chem.* **1961**, *17*, 215–221. [[CrossRef](#)]